

SUPPLEMENTARY INFORMATION

ARRHENIUS EQUATION

The ion migration has been modeled with the Arrhenius equation, usually employed to determine the temperature dependence of reaction rates. Here, the low frequency rate constant of the third semicircle represents the hopping rate, r_m :¹⁻⁵

$$r_m \propto \exp\left(-\frac{E_A}{k_B T}\right)$$

where k_B and T are Boltzmann constant and absolute temperature, respectively. A plot of $\ln(r_m)$ versus $1/T$ should give a straight line, from which the activation energy can be obtained from the slope.

Degree of hysteresis:

For the calculation of the degree of hysteresis we use a similar approach to the one proposed by Levine et al.² with slight modifications to the formula. The degree of hysteresis was calculated according with the formula

$$\text{Degree of hysteresis} \equiv 100 * \left(\frac{A_{Voc\ to\ Jsc} - A_{Jsc\ to\ Voc}}{A_{max}}\right) \quad (S1)$$

where A_{max} is the largest J-V curve area between backward and forward direction. The reason behind this formula is that for inverted perovskite solar devices it could be possible to observe inverted hysteresis, as it was the case for the majority of the cells reported in this work, where the forward scan has the highest performance. The degree of hysteresis obtained with this formula shows the ratio between J-V curves regardless of the scan direction and at the same time distinguishes between normal and inverted hysteresis. The nature of the inverted hysteresis for inverted perovskite solar cells is beyond the scope of this work.

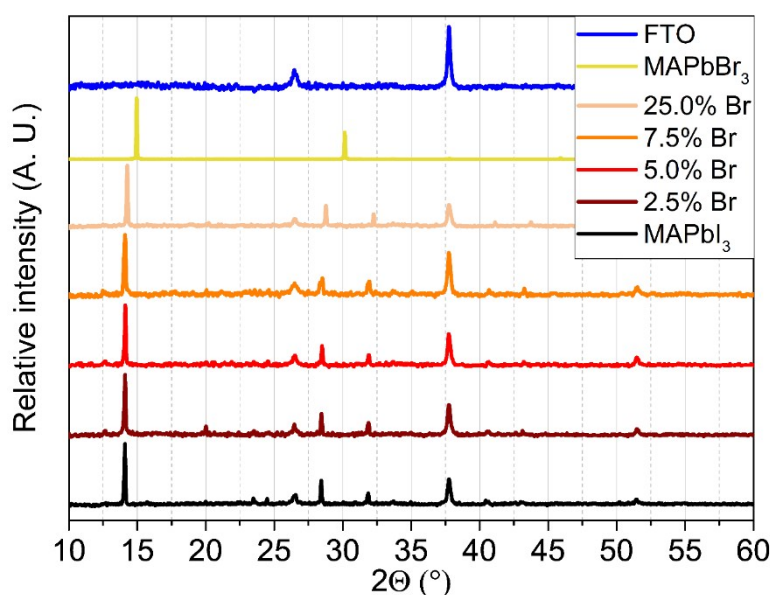


Figure S1. XRD measurements for perovskite films where the FTO peak is used as reference. The concentrations employed were 0.6 M for the perovskite solutions to ensure thinner films and to allow the underlying FTO peak to be observed. The

FTO peak position is independent of perovskite composition and allowed us to more accurately calculate peak displacement due to changes in perovskite composition.

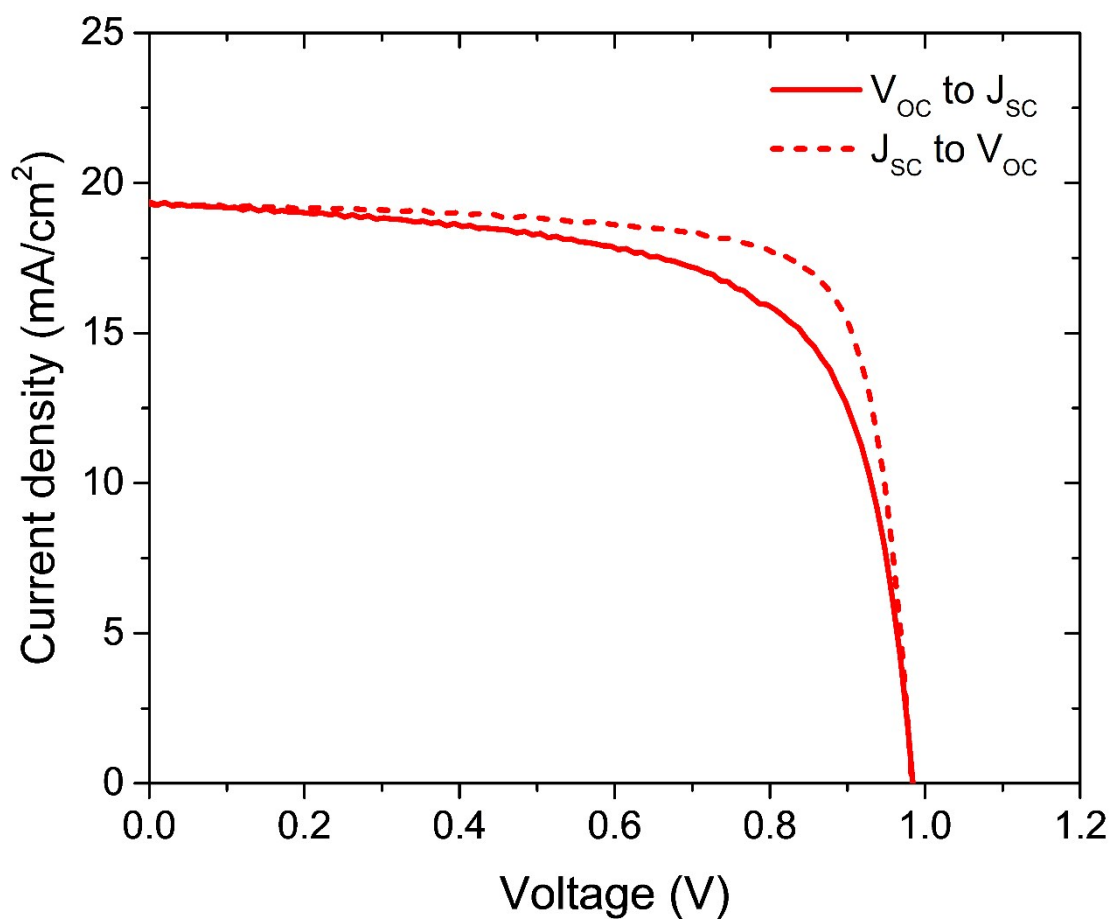


Figure S2. Solvent annealed inverted perovskite solar cell with 14.6% efficiency.

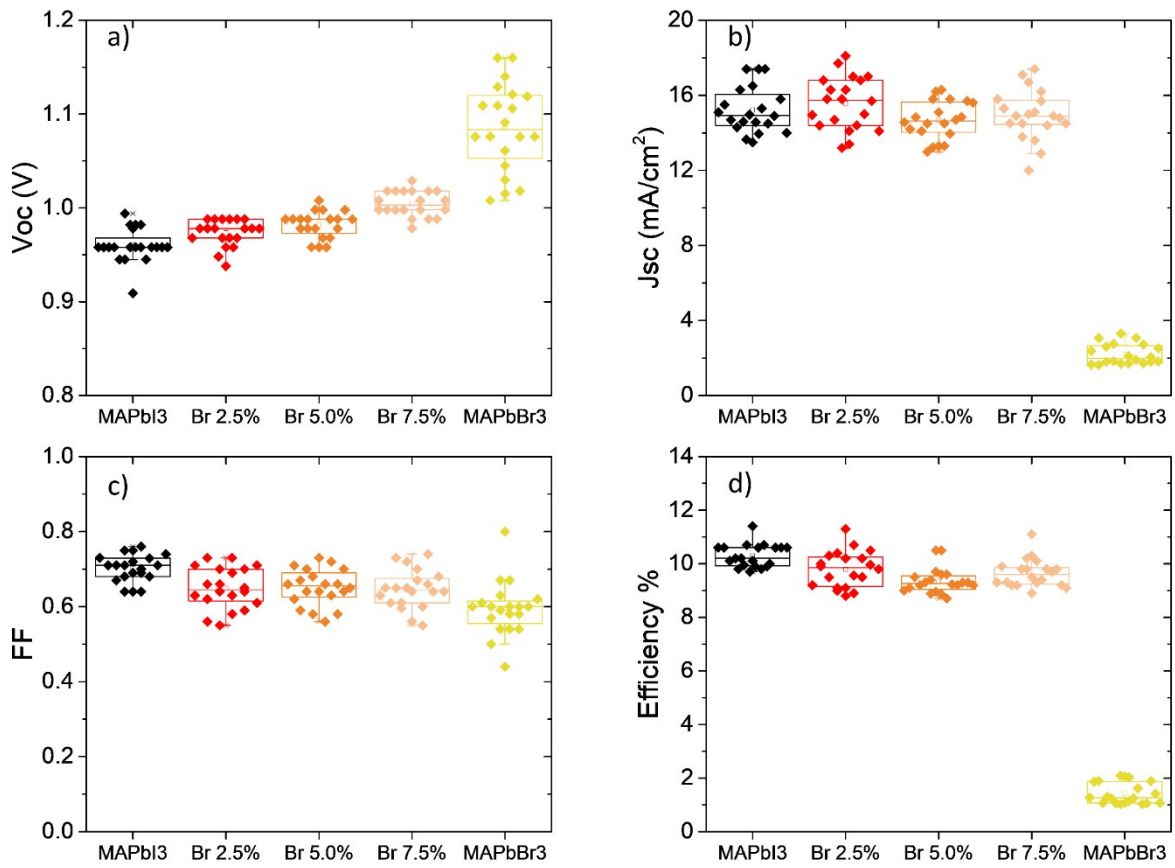


Figure S3. Photovoltaic parameters of perovskite solar cells as a function of bromide concentration: a) open circuit potential, b) short-circuit current density, c) fill factor and d) efficiency. The best 20 pixels for each configuration are displayed.

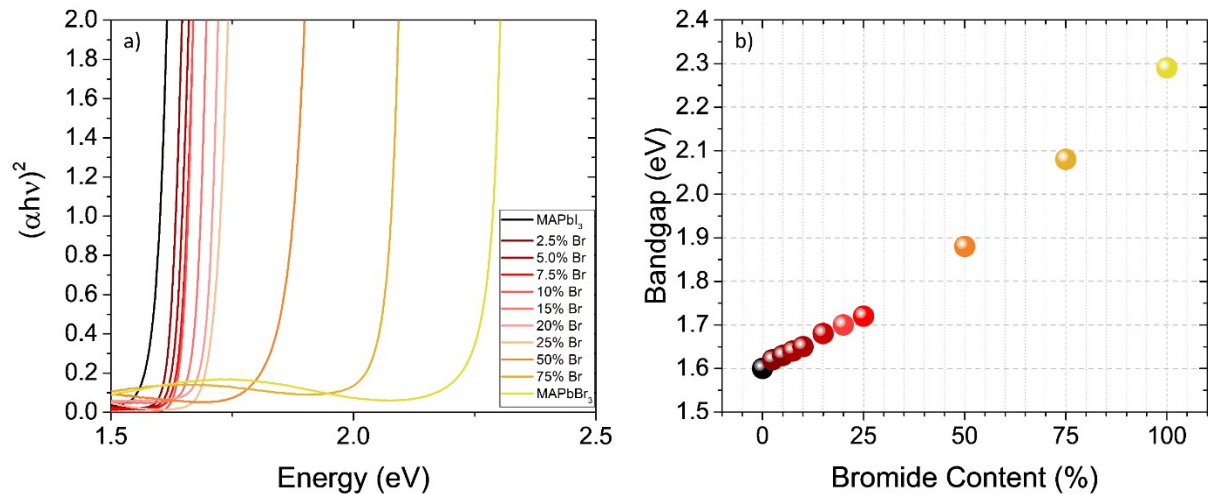


Figure S4. a) Tauc plot and b) bandgap of the perovskite as a function of bromide content, obtained via UV-Vis transmission and reflectance measurements.

Table S1. Energy bandgap values obtained for the perovskite material as a function of bromide content, obtained for direct allowed transitions.

Perovskite Composition	Bandgap (eV)
MAPbI ₃	1.6
MAPb(I _{0.975} Br _{0.025}) ₃	1.62
MAPb(I _{0.95} Br _{0.050}) ₃	1.63
MAPb(I _{0.925} Br _{0.075}) ₃	1.64
MAPb(I _{0.90} Br _{0.10}) ₃	1.65
MAPb(I _{0.85} Br _{0.15}) ₃	1.68
MAPb(I _{0.80} Br _{0.20}) ₃	1.70
MAPb(I _{0.75} Br _{0.25}) ₃	1.72
MAPb(I _{0.50} Br _{0.50}) ₃	1.88
MAPb(I _{0.25} Br _{0.75}) ₃	2.08
MAPbBr ₃	2.29

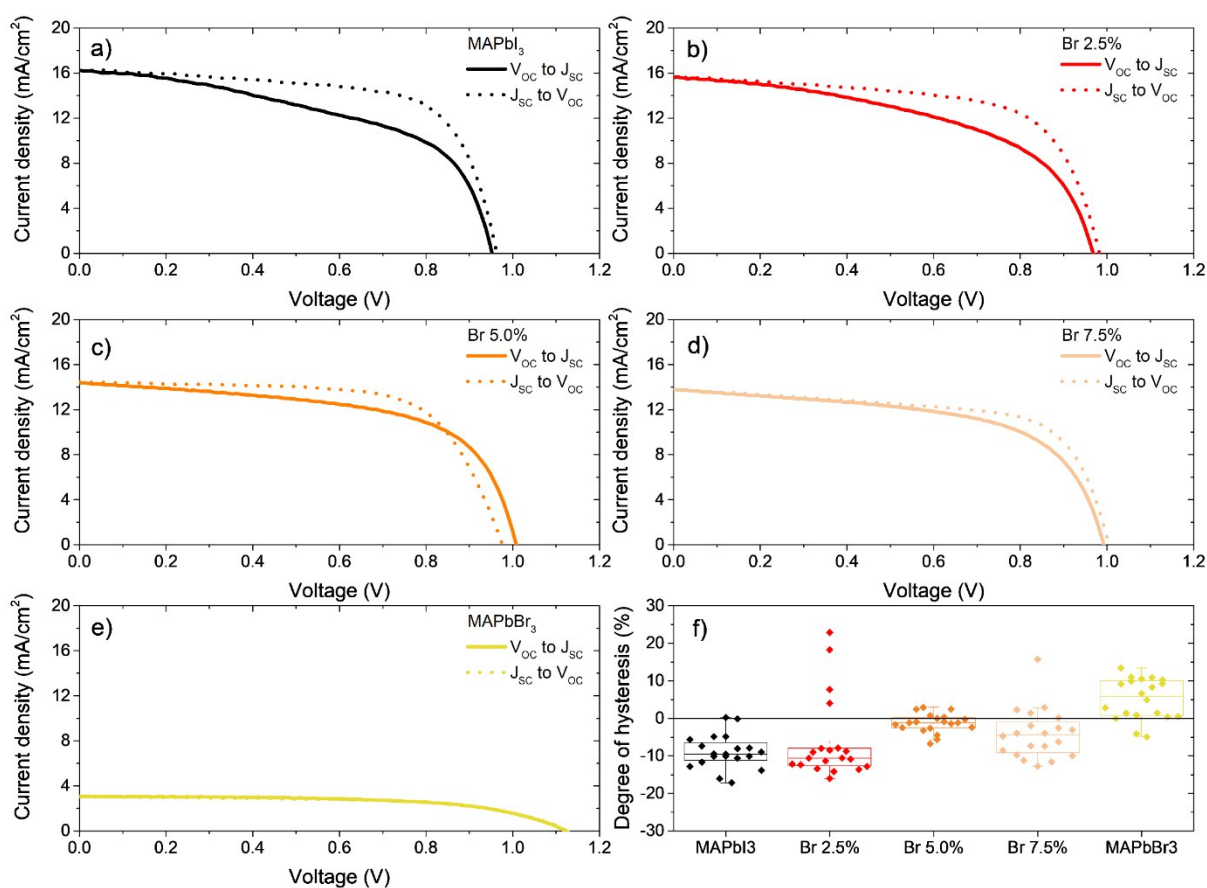


Figure S5. a-e) Representative J-V curves for perovskite solar cells with different bromide concentration. The scan direction is highlighted to show the inverted hysteresis. f) Degree of hysteresis at 1 sun illumination as a function of bromide content. The best 20 pixel values are displayed for each bromide concentration.

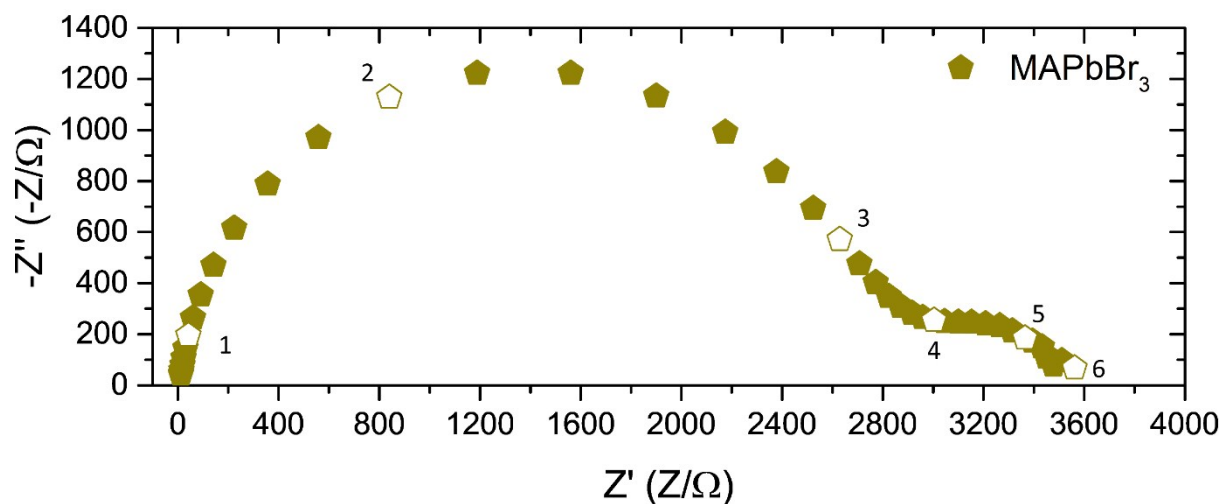


Figure S6. Nyquist plot for pure MAPbBr₃. Key frequency values are highlighted: 1 = 100 kHz, 2 = 10 kHz, 3 = 1 kHz, 4 = 100 Hz, 5 = 10 Hz and 6 = 1 Hz.

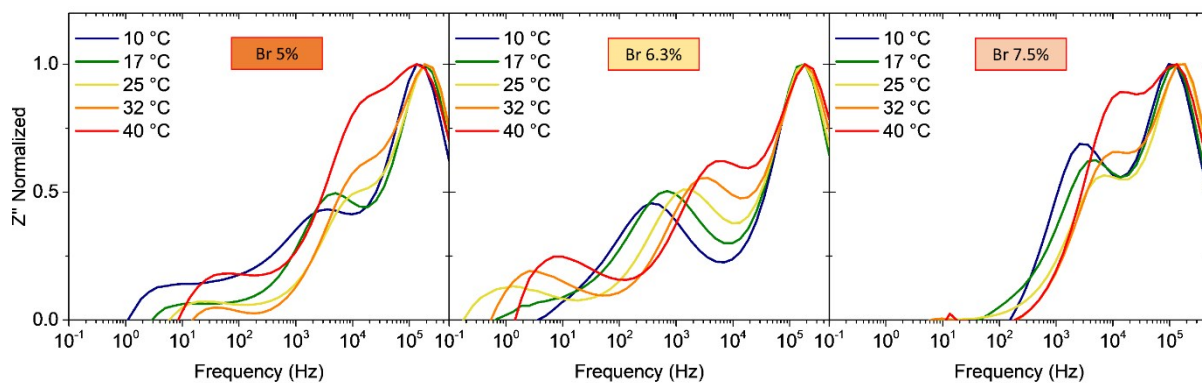


Figure S7. Cole plot of perovskite solar cells as a function of temperature and bromide concentration.

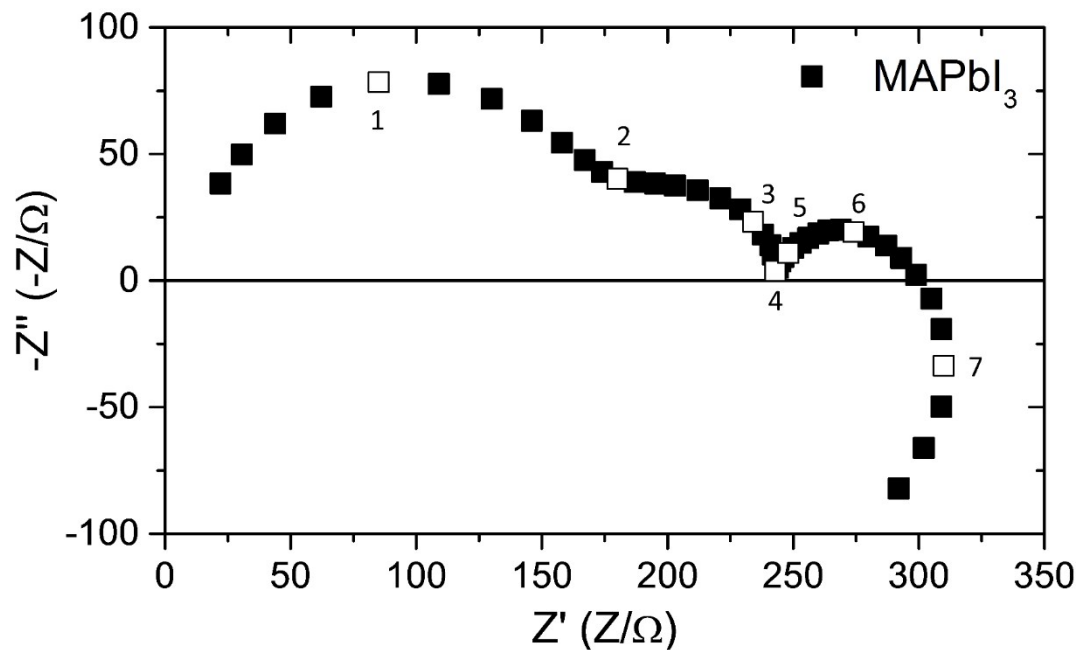


Figure S8. Nyquist plot for pure MAPbI₃ with a positive value of the imaginary component of the impedance at low frequencies. Key frequency values are highlighted: 1 = 100 kHz, 2 = 10 kHz, 3 = 1 kHz, 4 = 100 Hz, 5 = 10 Hz, 6 = 1 Hz and 7 = 100 mHz.

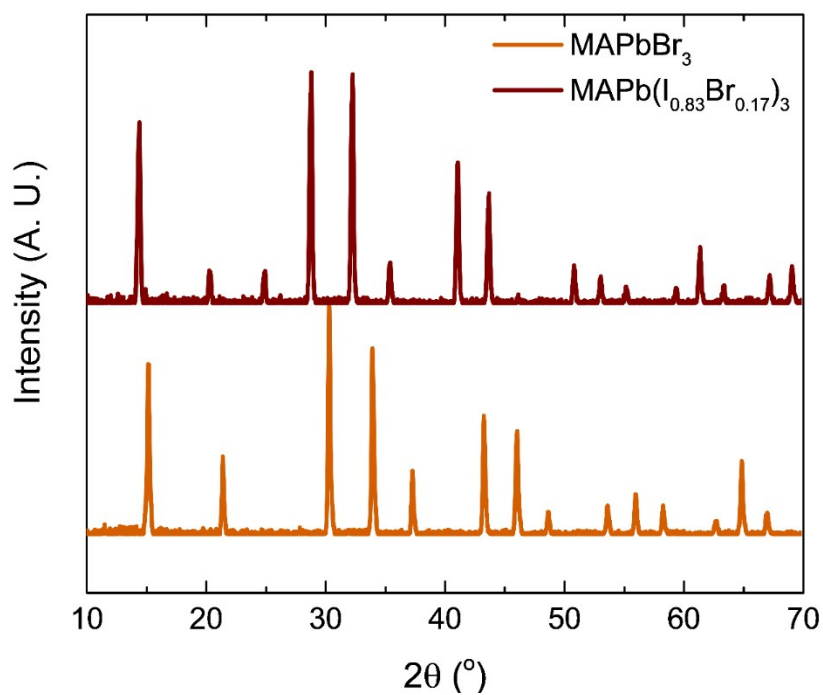


Figure S9. pXRD of MAPbBr_3 and $\text{MAPb}(\text{I}_{0.83}\text{Br}_{0.17})_3$ powders

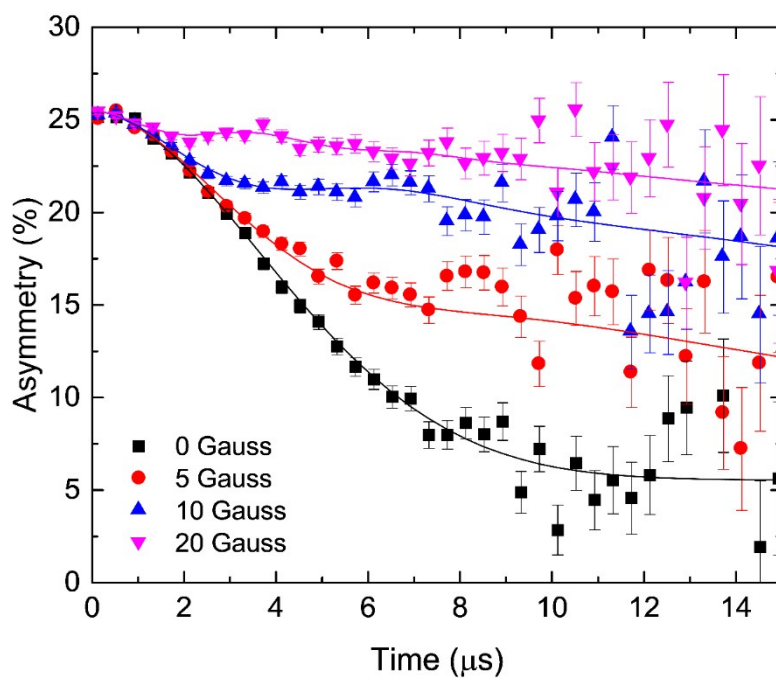


Figure S10. Raw muon data with fits to the dynamic Gaussian Kubo-Toyabe function (Equation 1).

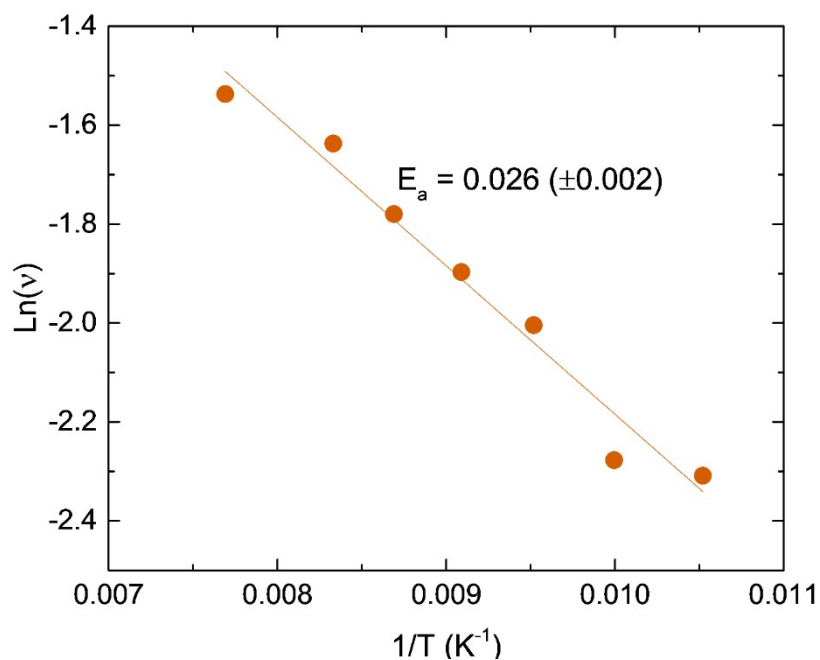


Figure S11. Activation energy related with cation dynamics for MAPbBr₃ obtained from muon spin relaxation.

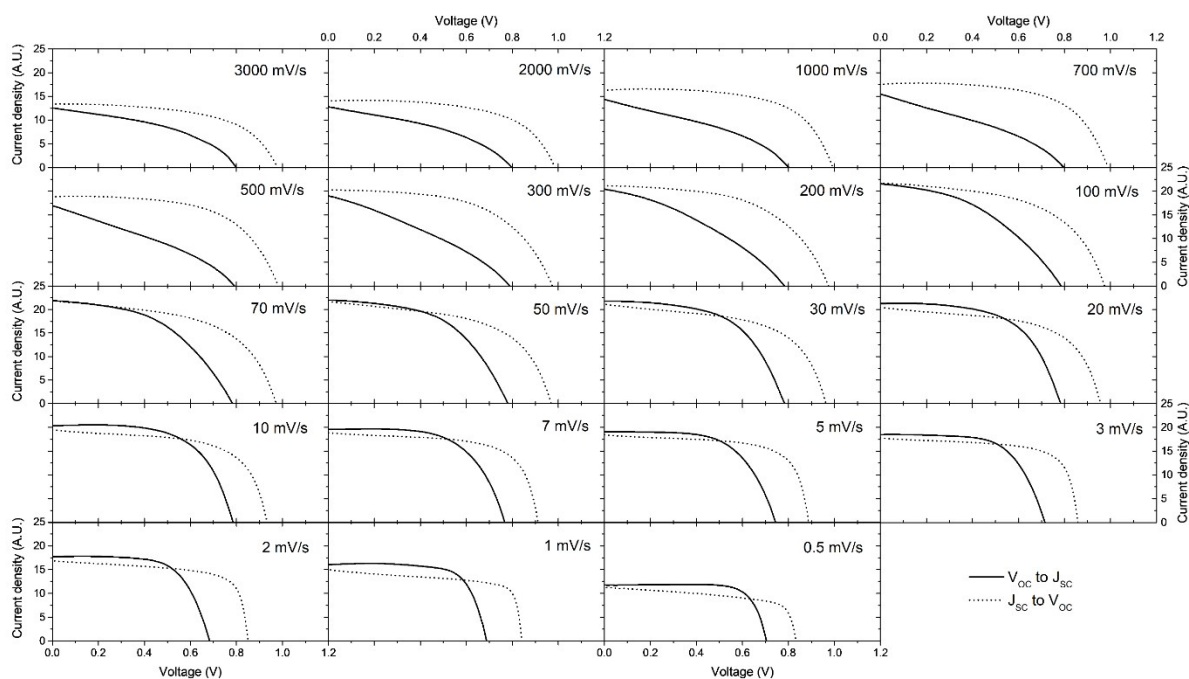


Figure S12. J-V curves for MAPbI₃ perovskite solar cells at different scan rates. The scan rates and scan direction employed are highlighted. The cells were measured under blue LED illumination (470 nm).

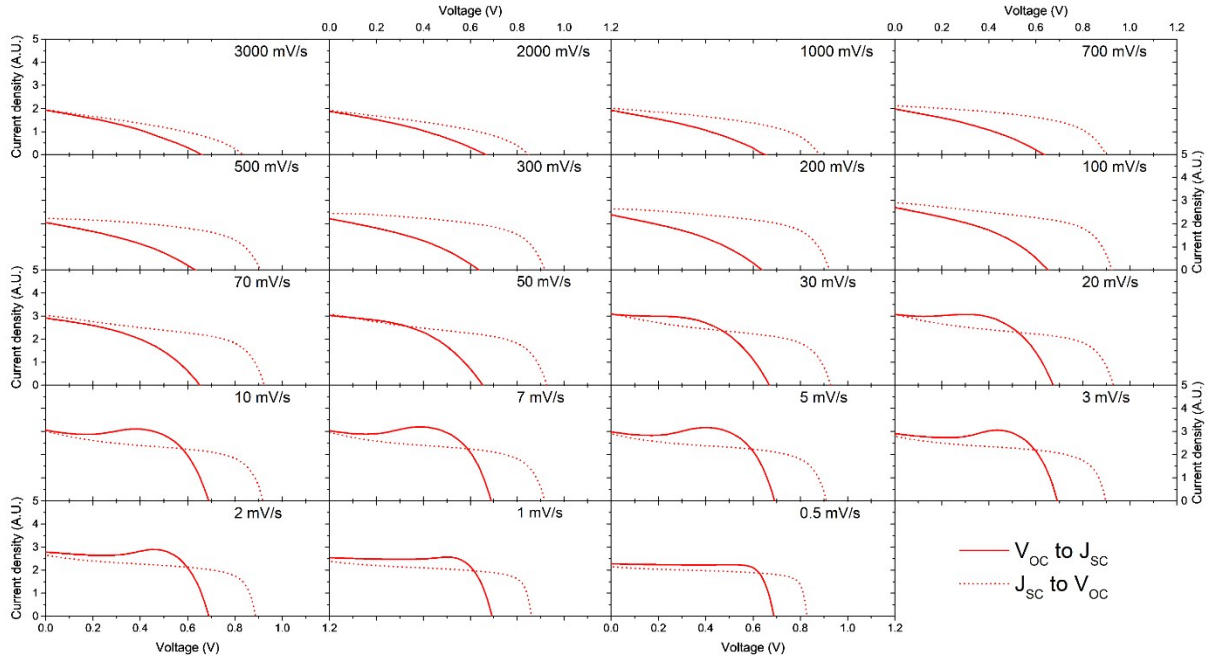


Figure S13. J-V curves for perovskite solar cells with 1.0% bromide content. The scan rates and scan direction employed are highlighted. The cells were measured under blue LED illumination (470 nm).

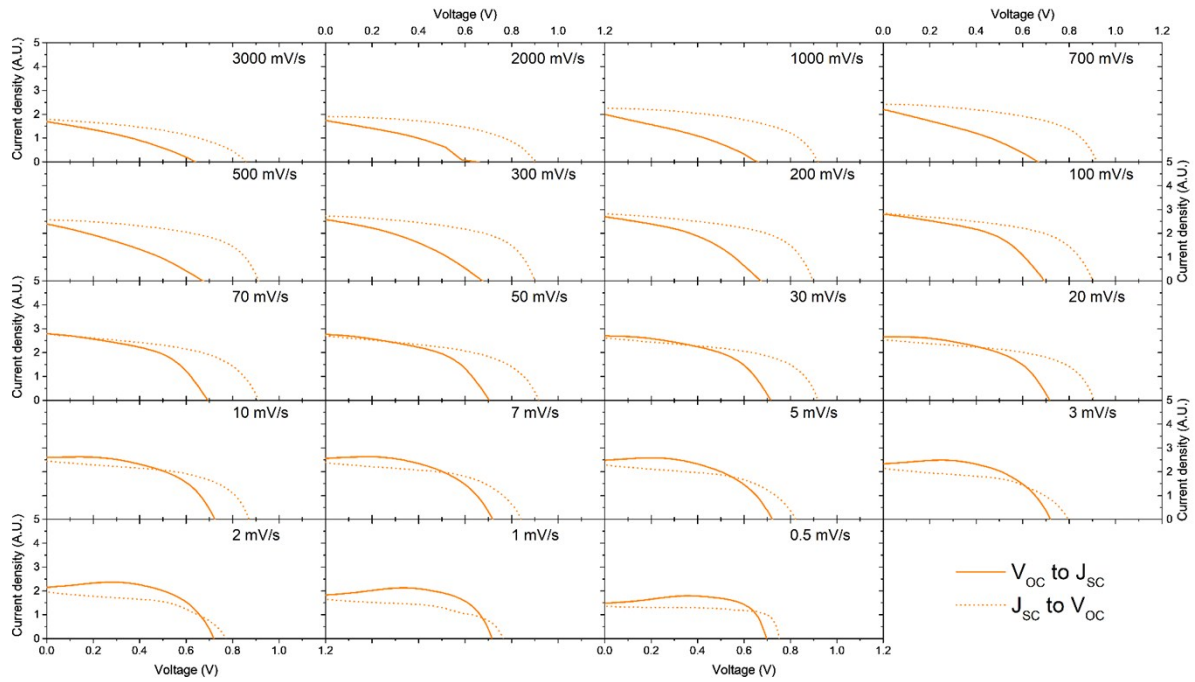


Figure S14. J-V curves for perovskite solar cells with 5.0% bromide content. The scan rates and scan direction employed are highlighted. The cells were measured under blue LED illumination (470 nm).

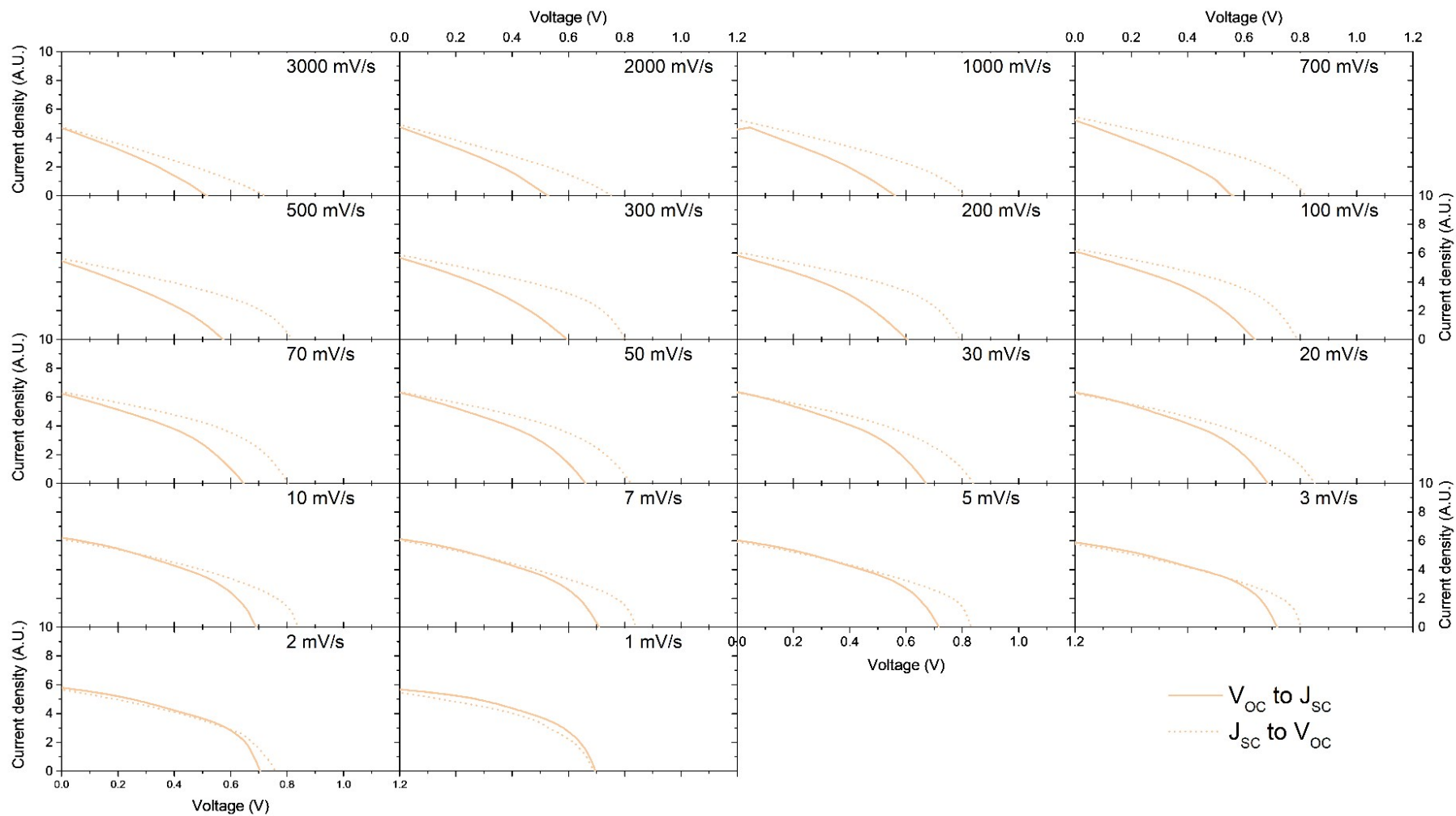


Figure S15. J-V curves for perovskite solar cells with 7.5% bromide content. The scan rates and scan direction employed are highlighted. The cells were measured under blue LED illumination (470 nm).

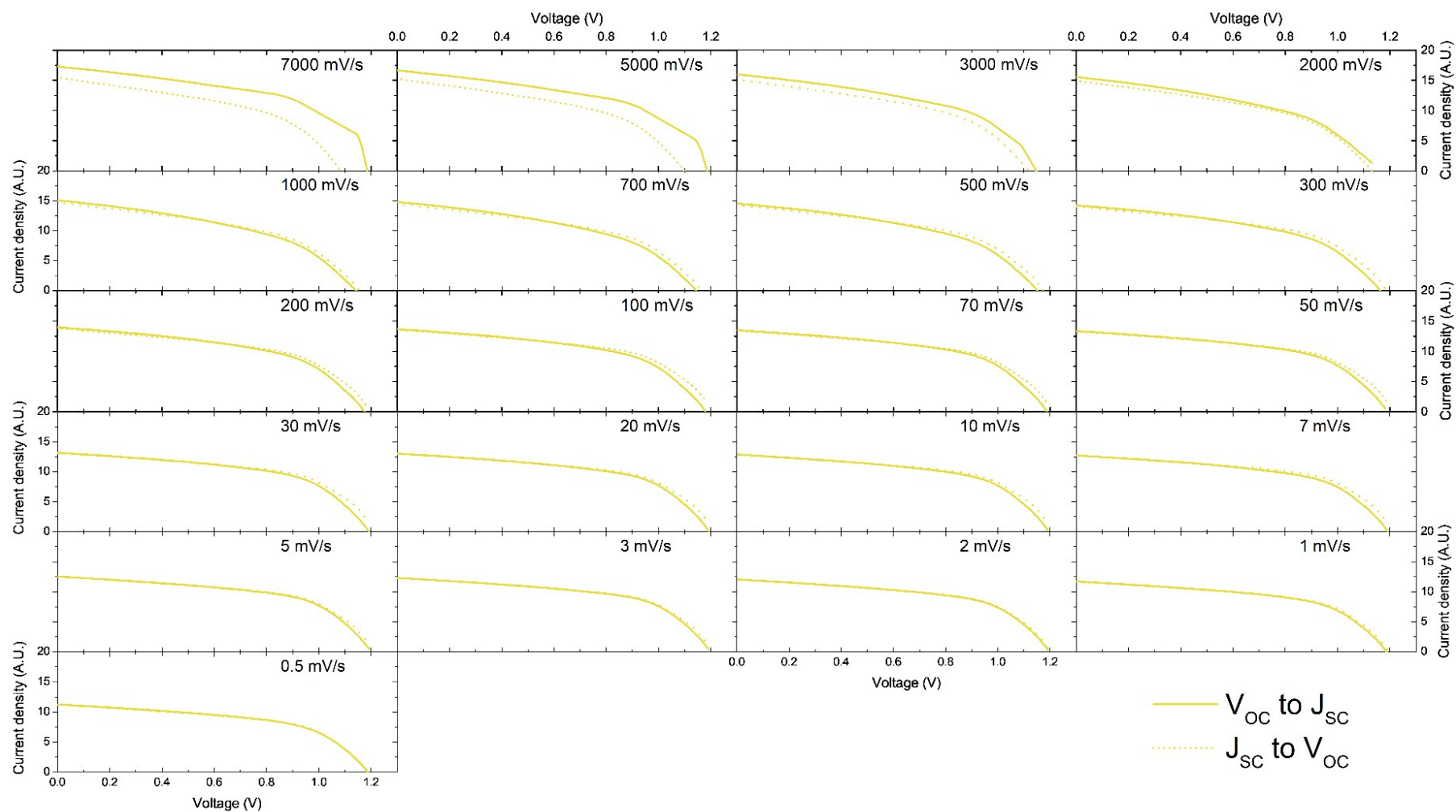


Figure S16. J-V curves for MAPbBr₃ perovskite solar cells. The scan rates and scan direction employed are highlighted. The cells were measured under blue LED illumination (470 nm).

REFERENCES

- 1 M. L. Petrus, J. Schlipf, C. Li, T. P. Gujar, N. Giesbrecht, P. Müller-Buschbaum, M. Thelakkat, T. Bein, S. Hüttner and P. Docampo, *Adv. Energy Mater.*, 2017, **7**, 1700264.
- 2 I. Levine, P. K. Nayak, J. T. W. Wang, N. Sakai, S. Van Reenen, T. M. Brenner, S. Mukhopadhyay, H. J. Snaith, G. Hodes and D. Cahen, *J. Phys. Chem. C*, 2016, **120**, 16399–16411.
- 3 S. Meloni, T. Moehl, W. Tress, M. Franckevicius, M. Saliba, Y. H. Lee, P. Gao, M. K. Nazeeruddin, S. M. Zakeeruddin, U. Rothlisberger and M. Graetzel, *Nat. Commun.*, 2016, **7**, 10334.
- 4 J. M. Azpiroz, E. Mosconi, J. Bisquert and F. De Angelis, *Energy Environ. Sci.*, 2015, **8**, 2118–2127.
- 5 A. Pockett, G. Eperon, N. Sakai, H. Snaith, L. M. Peter and P. J. Cameron, *Phys. Chem. Chem. Phys.*, 2017, **19**, 5959–5970.